Article

Fragmentation of Fiberlike Structures: Sonication Studies of Cylindrical Block Copolymer Micelles and Behavioral Comparisons to Biological Fibrils

Ge#rald Gue#rin, Hai Wang, Ian Manners, and Mitchell A. Winnik

J. Am. Chem. Soc., **2008**, 130 (44), 14763-14771 • DOI: 10.1021/ja805262v • Publication Date (Web): 11 October 2008

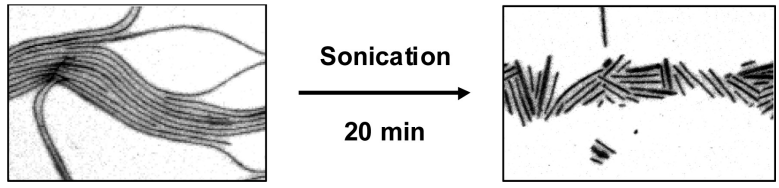

More About This Article

Additional resources and features associated with this article are available within the HTML version:

- Supporting Information
- Access to high resolution figures
- Links to articles and content related to this article
- Copyright permission to reproduce figures and/or text from this article

View the Full Text HTML

J|A|C|S
ARTICLES

Published on Web 10/11/2008

Fragmentation of Fiberlike Structures: Sonication Studies of Cylindrical Block Copolymer Micelles and Behavioral Comparisons to Biological Fibrils

Gérald Guérin,[†] Hai Wang,[†] Ian Manners,*[,‡] and Mitchell A. Winnik*[,†]

Department of Chemistry, University of Toronto, 80 St. George Street, Toronto, Ontario, Canada M5S3H6, and School of Chemistry, University of Bristol, BS8 1TS, England

Received July 8, 2008; E-mail: mwinnik@chem.utoronto.ca; Ian.Manners@bristol.ac.uk

Abstract: In alkane solvents, poly(isoprene-*b*-ferrocenyldimethylsilane) (PI-*b*-PFS) block copolymer forms fiberlike micelles, which show intriguing similarities with biological fibers such as amyloid fibers. Both systems exhibit fiber growth by a nucleated self-assembly mechanism and rapidly fragment upon exposure to the shear forces of ultrasonic irradiation. Sonication of PI-*b*-PFS cylindrical micelles was studied quantitatively by static light scattering and by electron microscopy. Both techniques are in excellent agreement and show that the weight-average length of sonicated micelles decreases as a function of sonication time. Simulation of the cleavage of micelles using different scission models shows that micelle fragmentation follows a Gaussian model and that the scission is highly dependent on micelle length, in contrast to DNA and polymer chain scission. We speculate that biological fibers, which are similar in length and rigidity to PFS block copolymer micelles, fragment by a similar mechanism when subjected to sonication.

Introduction

The formation of cylindrical or fiberlike structures through the self-assembly of macromolecules is a topic of widespread interest in a variety of different fields. For example, in the field of polymer materials, cylindrical micelles of PEO-PEP [PEO, poly(ethylene oxide); PEP, poly(ethylene-*alt*-propylene)], incorporated into epoxy resins, dramatically enhance their toughness.[1] In the field of biomimetic mineralization, cylindrical aggregates of a peptide−amphiphile have been employed as a fibrous scaffold for the directed formation of hydroxyapatite crystals.[2] For flow-intensive drug delivery, Discher and coworkers[3] demonstrated that cylindrical micelles are ideal in that they can orient and stretch in a flowing stream. In medicine, because of the key role of protein fibrils in Alzheimer's and other amyloidose diseases,[4,5] the formation and degradation of amyloid fibrils has been of particular interest. We have been interested in polyferrocenysilane (PFS) block copolymers.[6] These polymers form fiberlike micelles for a broad range of compositions in a variety of solvents that are selective for the non-PFS block. In this paper, we draw analogies between the formation and fragmentation mechanisms of PFS block copolymer micelles and amyloid fibrils. We show that one can obtain unique and important quantitative information about the sonication-induced fragmentation of fiberlike structures from the study of PFS block copolymer micelles.

Our study is made possible by the preparation of micelles that are nearly monodisperse in length. The building blocks are poly(isoprene-*b*-ferrocenylsilane) (PI-*b*-PFS) block copolymer molecules dissolved in hexane, a good solvent for polyisoprene but a poor solvent for polyferrocenysilane. We refer to the sample investigated here as PI_{264}-*b*-PFS_{48}, where the subscripts refer to the number-average degree of polymerization. These block copolymer micelles are interesting from a number of different points of view. PFS can be oxidized to a semiconducting state, offering the potential for semiconducting nanowires, and it can be pyrolyzed to yield a magnetic ceramic.[7,8] The rodlike micelles formed are rather rigid, with persistence lengths on the order of a few micrometers. When solutions of the micelles are sonicated, the structures fracture to yield fragments of similar thickness and lengths of 100−500 nm.

At present, PFS block copolymers are the only block copolymers known to self-assemble by a nucleated "living polymerization" mechanism, in which new macromolecules selectively condense on the ends of existing fibrils.[9] This is a process that is well documented for the growth of F-actin, as well as for a series of amyloids including synthetic human amylin and β-amyloid.[10−15] While there are many differences between PFS-block copolymer micelles and these natural

[†] University of Toronto.
[‡] University of Bristol.

(1) Dean, J. M.; Verghese, N. E.; Pham, H. Q.; Bates, F. S. *Macromolecules* **2003**, *36*, 9267–9270.
(2) Hartgerink, J. D.; Beniash, E.; Stupp, S. I. *Science* **2001**, *294*, 1684–1688.
(3) Dalhaimer, P.; Bates, F. S.; Discher, D. E. *Macromolecules* **2003**, *36*, 6873–6877.
(4) Dobson, C. M. *Nature* **2002**, *418*, 729–730.
(5) Dobson, C. M. *Nature* **2003**, *426*, 884.
(6) Guerin, G.; Raez, J.; Wang, X. S.; Manners, I.; Winnik, M. A. *Prog. Colloid Polym. Sci.* **2006**, *132*, 152–160.
(7) Wang, X. S.; Arsenault, A.; Ozin, G. A.; Winnik, M. A.; Manners, I. *J. Am. Chem. Soc.* **2003**, *125*, 12686–12687.
(8) Wang, X. S.; Liu, K.; Arsenault, A. C.; Rider, D. A.; Ozin, G. A.; Winnik, M. A.; Manners, I. *J. Am. Chem. Soc.* **2007**, *129*, 5630–5639.
(9) Wang, X. S.; Guerin, G.; Wang, H.; Wang, Y.; Manners, I.; Winnik, M. A. *Science* **2007**, *317*, 644–647.
(10) Goldsbury, C.; Kistler, J.; Aebi, U.; Arvinte, T.; Cooper, G. J. S. *J. Mol. Biol.* **1999**, *285*, 33–39.
(11) Ban, T.; Yamaguchi, K.; Goto, Y. *Acc. Chem. Res.* **2006**, *39*, 663–670.

structures, we choose to focus on the similarities, in the hopes of deepening our understanding of aspects of macromolecular self-assembly to form micrometer-long uniform fibers with nanometer thicknesses. For example, in vitro studies of the Sup35p prion-determining domain of the yeast *Saccharomyces cerevisiae*, consisting of the end (N) and middle (M) regions, show that this region undergoes a conformational change to form amyloid fibers in a process that closely parallels prion propagation in vivo.[16] These fibers are relatively rigid and easily fractured into short pieces by sonication. The rate of fiber formation of purified NM is dramatically increased by the addition of preformed short NM fibers.

Recent work from the Lindquist laboratory[17] has shown that amyloid growth for this system is primarily bidirectional, with soluble macromolecules condensing at both ends of preformed fibers. In these experiments, the sonicated fibers were first decorated with 1.4 nm gold nanoparticles and then used to seed fiber growth through the addition of soluble NM protein. Then the size of the gold nanoparticles was enlarged by catalytic gold deposition (see ref 17 for details). The resulting structures, shown as bright-field transmission electron microscopy (TEM) images in Figure 1A, were decorated with gold nanoparticles in the central portion of the fiber, demonstrating fiber growth from both ends.

In our laboratory, we carried out similar experiments with fiberlike micelles of PFS-P2VP [P2VP = poly(2-vinylpyridine)] in isopropyl alcohol−water mixtures.[18] The P2VP component was partially quaternized by treatment with methyl iodide to yield a cationically charged corona, followed by sonication of the micelles to form shortened structures. When additional PFS-P2VP dissolved in tetrahydrofuran (THF) was added to the solution, the fiberlike structures became elongated. Then these were treated with anionically charged gold nanoparticles (with surface-bound thioacetic acid groups), and the gold nanoparticles bound selectively to the central cationic part of the structure, shown in a dark-field TEM image in Figure 1B, establishing that nucleated growth was bidirectional. We find these similarities between the PFS block copolymer micelles and the amyloid fibers to be fascinating.

Here, we are interested in studying the response of rigid one-dimensional objects to shear stress induced by sonication. This method has been applied to double-stranded high molecular weight DNAs,[19] which were degraded to smaller size fragments without disturbing their double-helical conformation. Because explosive polymerization and recombination are often observed when F-actin[20] or amyloid fibrils[21,22] are sonicated, it is difficult to study their fragmentation quantitatively. This is a major advantage of PI-*b*-PFS micelles, which are more stable in solution.[8] In a previous study, we showed that when PI-*b*-PFS micelles were sonicated, the apparent hydrodynamic radius of the micelles decreased exponentially with sonication time and appeared to reach a limiting value.[9] Prior to the experiments reported here, there was no evidence that, like DNA, the inner structure of the micelles was not affected by ultrasound.[23] Moreover, while many studies of polymer degradation by ultrasound have been reported so far,[24−30] little is known about the process leading to the cleavage of rigid, micrometer-long micelles in solution.

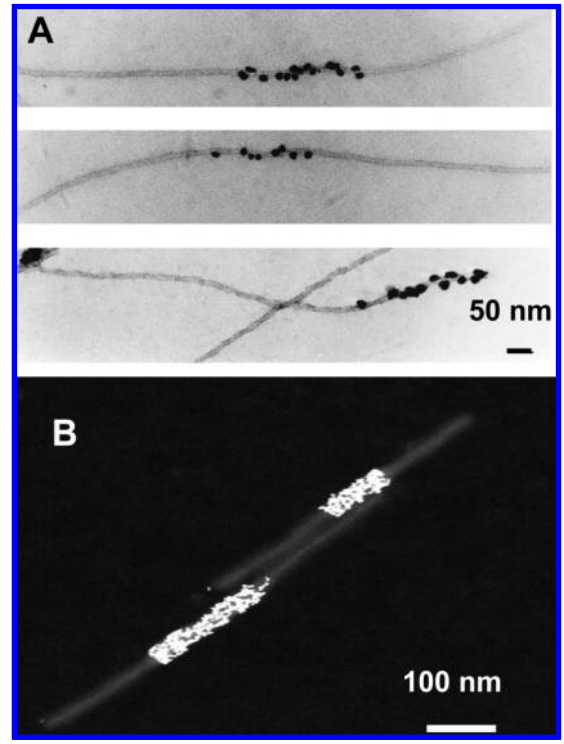

Figure 1. Comparison of (A) bright-field TEM image of gold-decorated NM fibers, obtained by seeded growth from NM protein fiber fragments from the Sup35p prion-determining domain [image from ref 17], with (B) dark-field TEM image of gold-decorated PFS-P2VP micelles, obtained by seeded growth from sonicated PFS-P2VP fragments [image from ref 18]. In both cases, the gold nanoparticles label the seed fragment. In panel A, one can see that while most of these protein fibers grow bidirectionally, some protein fibers grow in one direction. Figure 1A is reproduced with permission of the publisher.

In this paper, we present a study of the cleavage by ultrasound of PI-*b*-PFS cylindrical micelles using a combination of TEM and light scattering techniques. We show that the rate of cleavage dramatically increases with the length of PI_{264}-*b*-PFS_{48}

(12) Blackley, H. K. L.; Sanders, G. H. W.; Davies, M. C.; Roberts, C. J.; Tendler, S. J. B.; Wilkinson, M. J. *J. Mol. Biol.* **2000**, *298*, 833–840.
(13) Dobson, C. M. *Philos. Trans. R. Soc. London* **2001**, *B356*, 133–145.
(14) Sunde, M.; Blake, C. C. F. *Adv. Protein Chem.* **1997**, *50*, 123–159.
(15) Booth, D. R.; Sunde, M.; Beliotti, V.; Robinson, C. V.; Hutchinson, W. L.; Fraser, P. E.; Hawkins, P. N.; Dobson, C. M.; Radford, S. E.; Blake, C. C. F.; Pepys, M. B. *Nature* **1997**, *385*, 787–793.
(16) Serio, T. R.; Cashikar, A. G.; Kowal, A. S.; Sawicki, G. J.; Moslehi, J. J.; Serpell, L.; Arnsdorf, M. F.; Lindquist, S. L. *Science* **2000**, *289*, 1317–1321.
(17) Scheibel, T.; Kowal, A. S.; Bloom, J. D.; Lindquist, S. L. *Curr. Biol.* **2001**, *11*, 366–369.
(18) Wang, H.; Lin, W.; Fritz, K. P.; Scholes, G. D.; Winnik, M. A.; Manners, I. *J. Am. Chem. Soc.* **2007**, *129*, 12924–12925.
(19) Tanigawa, M.; Suzuto, M.; Fukudome, K.; Yamaoka, K. *Macromolecules* **1996**, *29*, 7418–7425.
(20) Hama, H.; Kasai, M.; Maruyama, K.; Noda, H. *Biochim. Biophys. Acta* **1969**, *194*, 470–477.
(21) Binger, K. J.; Pham, C. L. L.; Wilson, L. M.; Bailey, M. F.; Lawrence, L. J.; Schuck, P.; Howlett, G. J. *J. Mol. Biol.* **2008**, *376*, 1116–1129.
(22) Ohhashi, Y.; Kihara, M.; Naiki, H.; Goto, Y. *J. Biol. Chem.* **2005**, *280*, 32843–32848.
(23) Massey, J.; Power, K. N.; Manners, I.; Winnik, M. A. *J. Am. Chem. Soc.* **1998**, *120*, 9533–9540.
(24) Ballauff, M.; Wolf, B. A. *Macromolecules* **1984**, *17*, 209–216.
(25) Kuhn, K. J.; Hellmann, G. P. *J. Polym. Sci., Part B: Polym. Phys.* **1990**, *28*, 2165–2182.
(26) Netopilik, M.; Kubin, M.; Schultz, G.; Vohlidal, J.; Kossler, I.; Kratochvil, P. *J. Appl. Polym. Sci.* **1990**, *40*, 1115–1130.
(27) Tayal, A.; Khan, S. A. *Macromolecules* **2000**, *33*, 9488–9493.
(28) Buchholz, B. A.; Zahn, J. M.; Kenward, M.; Slater, G. W.; Barron, A. E. *Polymer* **2004**, *45*, 1223–1234.
(29) Lee, K.; Kim, C. A.; Lim, S. T.; Kwon, D. H.; Choi, H. J.; Jhon, M. S. *Colloid Polym. Sci.* **2002**, *280*, 779–782.
(30) Madras, G.; McCoy, B. J. *Chem. Eng. Sci.* **1997**, *52*, 2707–2713.

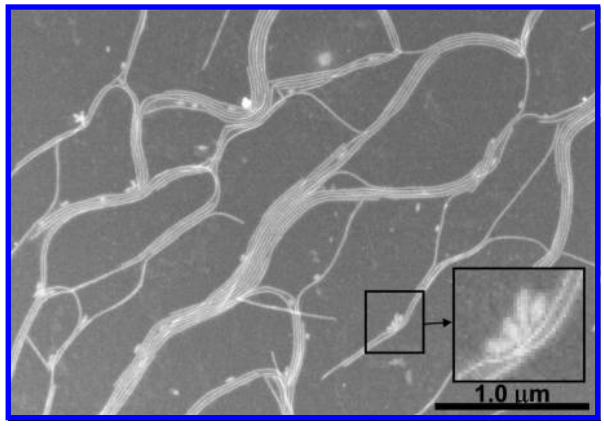

Figure 2. Dark-field TEM image of PI_{264}-*b*-PFS_{48} micelles prepared by heating a solution in *n*-hexane followed by slow cooling to room temperature. Note the presence of small amounts of "debris", which are amorphous aggregates of the polymer not incorporated into the cylindrical micelles.

micelles and that fracture occurs preferentially near the center of the micelle. Because of the structural analogy between these micelles and amyloid fragments, we speculate that fragmentation takes place by a similar mechanism for these protein fibers. We also compare the mechanism involved in the breakage of the micelles with the mechanism involved for the fragmentation of polymer chains and DNA strands subjected to ultrasound.

Results and Discussion

In a selective solvent, block copolymers self-assemble to form well-defined micellar aggregates, which organize in various morphologies, such as spheres, cylinders, and more complex architectures.[31−33] When both blocks are amorphous ("coil−coil" block copolymers), spheres are the most probable structures, while other structures will be formed for a narrow range of block ratios.[32] However, in the case of rod−coil or crystalline−coil block copolymers, elongated structures are more accessible.[34−37] Polyferrocenylsilane diblock copolymers are unique in their ability to form extremely long and rigid cylindrical micelles for a wide range of block compositions and block ratios.[23,38−40] The key structural feature associated with formation of these rodlike structures is the semicrystalline nature of the micelle core formed by the PFS block. In the following section, we compare the contour length distribution (CLD) of PI_{264}-*b*-PFS_{48} micelles with that of cylindrical micelles formed from block copolymers in which both blocks are amorphous.

Contour Length Distribution of PI_{264}-*b*-PFS_{48} Micelles. The contour length distribution (CLD) of cylindrical micelles formed from coil−coil diblock copolymers have been recently evaluated by LaRue et al.[41] for poly(styrene-*b*-isoprene) (PS_{392}-*b*-PI_{153}) diblock copolymers in heptane and by Dalhaimer et al.[3] for poly(butadiene-*b*-ethylene oxide) (PBD_{45}-*b*-PEO_{55}) diblock copolymers in water. PBD-PEO micelles were shown to form stable cylindrical assemblies stabilized by the PEO corona and with a broad CLD, well described by a model presented by Israelachvili[42] for one-dimensional micelles formed under equilibrium conditions. The PS-PI micelles were formed under conditions approximating equilibrium control, but then the glassy PS core of the micelles became kinetically frozen in heptane solution at room temperature. These wormlike micelles were also highly polydisperse, with a CLD ranging from 0.2 to 12 μm. In contrast, several PFS diblock copolymer samples, with polydimethylsiloxane[40] and polyisoprene[9] as the coblock, yielded much narrower CLDs.

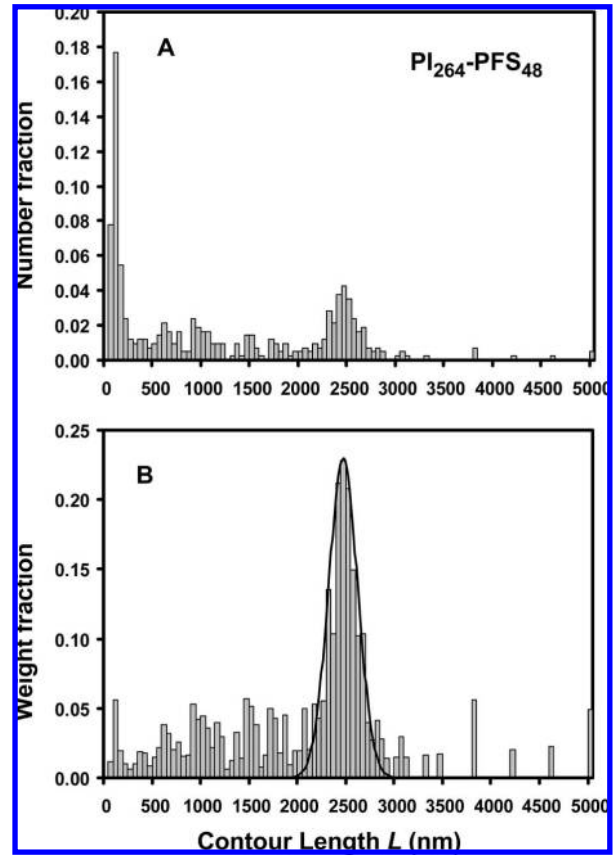

Figure 3. (A) Number and (B) weight length frequency of PI_{264}-*b*-PFS_{48} micelles prepared in *n*-hexane as described in the caption to Figure 2. The main peak apparent in panel B can be well represented by a Gaussian distribution: $F_w(L) = \exp[-(L - L_w)^2/(2\sigma^2)]$ with $L_w = 2450$ nm with a fwhm of 350 nm.

To place our studies of micelle sonication on a firm footing, we begin by examining, by light scattering and TEM, the CLD of PI_{264}-*b*-PFS_{48} micelles formed by heating a solution of the polymer (0.06 mg/mL in hexane) for 80 min. at 70 °C followed by slow cooling back to room temperature (21 °C). A representative TEM micrograph of a sample prepared in this way is shown in Figure 2. The image was obtained in the *z*-contrast (dark-field) mode, in which electron-rich objects

(31) Rodriguez-Hernandez, J.; Checot, F.; Gnanou, Y.; Lecommandoux, S. *Prog. Polym. Sci.* **2005**, *30*, 691–724.
(32) Zhulina, E. B.; Adam, M.; LaRue, I.; Sheiko, S. S.; Rubinstein, M. *Macromolecules* **2005**, *38*, 5330–5351.
(33) Jain, S.; Bates, F. S. *Science* **2003**, *300*, 460–464.
(34) Wang, H.; Wang, H. H.; Urban, V. S.; Littrell, K. C.; Thiyagarajan, P.; Yu, L. *J. Am. Chem. Soc.* **2000**, *122*, 6855–6861.
(35) Wang, H.; You, H. W.; Jiang, P.; Yu, L.; Wang, H. H. *Chem.—Eur. J.* **2004**, *10*, 986–993.
(36) Du, Z. X.; Xu, J.-T.; Fan, Z.-Q. *Macromolecules* **2007**, *40*, 7633–7637.
(37) Lazzari, M.; Scalarone, D.; Vazquez-Vazquez, C.; Lopez-Ouintela, M. A. *Macromol. Rapid Commun.* **2008**, *29*, 352–357.
(38) Raez, J.; Manners, I.; Winnik, M. A. *J. Am. Chem. Soc.* **2002**, *124*, 10381–10395.
(39) Massey, J. A.; Temple, K.; Cao, L.; Rharbi, Y.; Raez, J.; Winnik, M. A.; Manners, I. *J. Am. Chem. Soc.* **2000**, *122*, 11577–11584.
(40) Guerin, G.; Raez, J.; Manners, I.; Winnik, M. A. *Macromolecules* **2005**, *38*, 7819–7827.
(41) LaRue, I.; Adam, M.; da Silva, M.; Sheiko, S. S.; Rubinstein, M. *Macromolecules* **2004**, *37*, 5002–5005.
(42) Israelachvili, J. *Intermolecular and Surface Forces*, 2nd ed.; Academic Press: London, 1992; p 359.

appear bright. Long cylindrical structures of uniform width (ca. 20 nm) can be seen in the image, with lengths up to about 2 μm. In addition, one can also see small amounts of "debris", small odd-shaped aggregates not incorporated into the cylindrical micelles. As we describe below, these objects represent a significant fraction of the number of objects present in the image but become much less significant when one considers the weight length distribution of the objects. An interesting feature of amorphous flowerlike structures can be seen at higher magnification in the lower right of the image. Very similar features appeared in TEM images of a sample of PFS-P2VP dissolved in ethanol in the course of a slow morphological evolution from initially formed amorphous spherical micelles to long, uniform cylindrical micelles.[43] Over time (up to a year for this polymer−solvent combination), the fiberlike structures became longer and these structures disappeared, leading to the suggestion that they were amorphous aggregates that slowly dissolved, followed by the addition of these polymer molecules to the ends of existing fibers.

Figure 3A shows the number length frequency of the micelles measured by analysis of several TEM images taken from the same grid as the sample shown in Figure 2. We evaluated the contour length distribution of micelles based on the measurement of more than 400 micelles in these images. The number frequency representation highlights the presence of small objects in the sample and exhibits a peak around 100 nm, but one can also observe a second peak centered around 2500 nm.

To compare the results obtained by TEM image analysis with light scattering results, we also plot, in Figure 3B, the weight length frequency of the micelles, F_w, which was calculated as follows:

$$F_w(L_i) = \frac{L_i N_i}{\sum_i L_i N_i} \quad (1)$$

where N_i is the number of micelles (or aggregates) of length L_i. With such a plot, more representative of the weighted values provided by light scattering, one can see that the small objects become nearly negligible compared to the larger population. Analysis of the distribution presented in Figure 3B in terms of eq 1 yields $L_w^{TEM} = 2080$ nm, showing that the shorter structures seen in the TEM micrograph (Figure 2) make only a tiny contribution to the calculated value of L_w. This value is likely to be somewhat smaller than the true value of L_w because it does not take into account a small fraction of micelles longer than 2 μm that extend beyond the edges of the images analyzed. The main contribution of the micelle population is well-fitted by a narrow Gaussian distribution centered at $L_w^{Gauss} = 2450$ nm [with a full width at half-maximum (fwhm) of ca. 350 nm].

This narrow distribution in the weight length frequency was confirmed by a study of the same solution by static light scattering. Figure 4 shows a Holtzer−Casassa[44,45] plot of $qR_\theta/\pi M_0 Kc$, plotted as a function of q, of the sample used for the TEM study. This plot highlights the presence of elongated structures in the solution, because such objects exhibit a plateau at high q. By plotting the data in this way, the magnitude of the plateau value directly gives the number of polymer molecules per unit length ($N_{agg/L} \approx 3$/nm). One can also observe

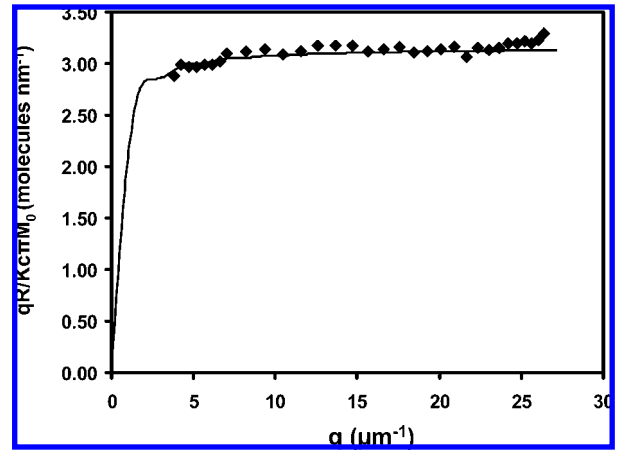

Figure 4. Plot of $qR/\pi KCM_0$ versus q for a solution of PI_{264}-*b*-PFS_{48} micelles in hexane ($c = 0.06$ mg/mL) taken from the same sample shown in Figure 2.

that the sample approaches its plateau value at relatively low values of q, as expected for solutions containing extremely long rods. [46] Another striking feature of the plot in Figure 4 is the presence of oscillations in the data, which indicate that the system is monodisperse in length. This feature is confirmed by the fit of the data as well as by the narrow length distribution seen in Figure 3B. The slight upturn in the data in the high q range is most likely due to back-reflection of light at high angles induced by the presence of such large objects. The solid line represents the best fit of the data to

$$f(q) = qP(q)M_w M_0 \pi \quad (2)$$

where M_w is the weight-average molecular weight of the micelle, M_0 is the weight-average molecular weight of PI-*b*-PFS diblock copolymer ($M_0 = 32\,000$ g/mol), $P(q)$ is the form factor used for thin rigid rods monodisperse in length:

$$P(q) = \frac{2}{qL}\int_0^{qL} \frac{\sin(qL)}{qL}\, d(qL_w) - \left[\frac{2}{qL}\sin\left(\frac{qL}{2}\right)\right]^2 \quad (3)$$

and L is the micelle length. In eqs 2 and 3, M_w and L are two fitting parameters.

Because the scattering intensity of a particle is related strongly to its size, objects such as the small aggregates seen in Figure 3 do not contribute significantly to the SLS data in Figure 4. The weight-average length of the micelles, $L_w^{SLS} = 2440$ nm, obtained from the fitting of the static light scattering data is in excellent agreement with the narrow Gaussian distribution centered at $L_w^{Gauss} = 2450$ nm representing the micelle population in Figure 3B.

Sonication and Fragmentation. Numerous studies have been performed on the degradation of polymer chains when submitted to shear stress, such as freeze−thaw cycles, sonication, or elongational flow experiments.[47−50] Those studies were aimed at understanding the mechanism of the fracture process and led to models that can be applied to different distributions of fracture sites along the chain. On the basis of work by Basedow and

(43) Shen, L.; Wang, H.; Guerin, G.; Wu, C.; Manners, I.; Winnik, M. A. *Macromolecules* **2008**, *41*, 4380–4389.
(44) Holtzer, A. *J. Polym. Sci.* **1955**, *17*, 432–434.
(45) Casassa, E. F. *J. Chem. Phys.* **1955**, *23*, 596–597.
(46) Schmidt, M.; Paradossi, G.; Burchard, W. *Makromol. Chem. Rapid Commun.* **1985**, *6*, 767–772.
(47) Basedow, A. M.; Ebert, K. H. *Adv. Polym. Sci.* **1977**, *22*, 83–148.
(48) Harrington, R. E.; Zimm, B. H. *J. Polym. Sci.* **1965**, *69*, 161–175.
(49) Basedow, A. M.; Ebert, K. H.; Ederer, H. J. *Macromolecules* **1978**, *11*, 774–781.
(50) Odell, J. A.; Muller, A. J.; Narh, K. A.; Keller, A. *Macromolecules* **1990**, *23*, 3092–3103.

Ebert,[47] Ballauff and Wolf[51] calculated the resulting distribution of polymer chains that undergo cleavage in different ways: random fracture with equal probability (model I), central scission (model II), or fracture with a Gaussian distribution of probabilities centered in the middle of the chain (model III). They observed that the final distribution of chain lengths depends on the scission process. In all situations, they noted that the polydispersity index (PDI) of the degraded sample reaches a plateau value that does not depend on the distribution of the polymer chain prior to degradation. Polymers with a broad PDI will have a narrower PDI following shear degradation. Elongational flow tends to fracture chains in the middle. Buchholz et al.[28] used the shear stress via elongated flow to obtain narrow-disperse polymers, which are hard to achieve in any other way. The behavior of DNA under stress has also generated a lot of interest.[47,52−55] Recently Tanigawa et al.[19] studied the sonication of double-stranded DNA. These authors proposed two other models to describe the cleavage of DNA strands. They considered cases where chains could not break in the vicinity of the ends. As a consequence, the molecular weight of the broken chains would reach a plateau value.

As we mentioned above, it is difficult to study directly the fragmentation of biological fibers subjected to ultrasonic waves. First, it remains a challenge to prepare samples with a narrow length distribution so that quantitative models of sonication can be tested. Second, such studies are complicated because those fibers can spontaneously break apart even without external stimulus.[56] In addition, sonication triggers both breakage and polymerization of amyloid and actin fibers.[20−22,57,58] In contrast, cylindrical block copolymer micelles are normally much more stable. Yan and Liu[59] examined the effects of sonication on chemically cross-linked cylindrical micelles. These authors used a Zimm plot analysis of their static light scattering data, which allowed them to infer that the weight-average molecular weight of the sonicated micelles was proportional to their weight-average length determined by TEM. We have shown that, following sonication, PFS diblock copolymer micelles form fragments whose lengths do not change over periods of days to weeks to months.[9,23] In the experiments we describe below, we take advantage of the narrow CLD of the micelles formed as shown in Figures 3 and 4. These micelles fragment when they are subjected to sonication, and the resulting distributions were determined by a combination of light scattering and TEM measurements.

SLS Studies of Micelle Scission. In Figure 5, we present Holtzer−Casassa plots of $qR_\theta/\pi M_0 Kc$, as a function of q, for nine sonication times, starting from the as-prepared micelle solution up to 40 min of sonication. Note that the oscillations present in the data of the sample before sonication (0 s) cannot be observed even after only 10 s of sonication (second curve from the top). This is an indication that the micelles are now polydisperse in length, due to the application of shear stress on the micelles.

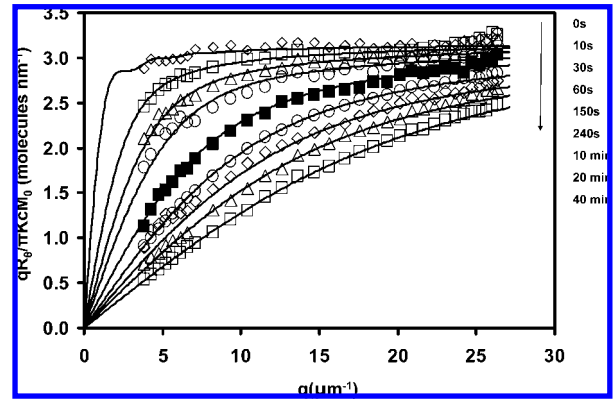

Figure 5. Plot of $qR/\pi KCM_0$ versus q of PI_{264}-*b*-PFS_{48} micelles at nine sonication times ranging from 0 s (upper curve) to 40 min (lower curve). The solid lines correspond to the best fit of the data. The sample concentration was $c = 0.06$ mg/mL.

Table 1. Main Characteristics Determined by SLS for Micelle Samples

sonication time	0 s	10 s	30 s	60 s	150 s	240 s	10 min	20 min	40 min
L_w (nm)	2440	1000	650	500	330	240	220	170	130
$z = 1/[(L_w/L_n) - 1]$	∞	5	5	5	3	3	3	3	3
$N_{agg/L}$	3.2	3.2	3.2	3.2	3.2	3.2	3.2	3.2	3.4

The samples subjected to brief sonication clearly approach a plateau at high q. As the sonication time increased, they approached their plateau at higher q values. For longer sonication times (>140 s), the data do not reach the plateau for accessible q values. This behavior is typical of a solution of micelles decreasing in length as the sonication time increases. To fit these data, the polydispersity in length of the micelles was taken into account by incorporating a Zimm−Schulz distribution into eq 2:

$$w(L) = \frac{b^{z+1}}{z!} L^z e^{-bL} \tag{4}$$

Here $b = (z + 1)/L_w$, and z is the dispersion parameter ($z = 1/[(L_w/L_n) - 1]$). For micelles monodisperse in length, z is infinite, whereas z decreases when the polydispersity increases. While the presence of the plateau is clearly evident only in the four uppermost curves, the plateau value could be obtained as a fitting parameter, allowing us to calculate the number of polymer molecules per unit length ($N_{agg/L}$) for all sonication times. The solid lines in Figure 5 correspond to the best fit of the data, and the parameters deduced from the data analysis are summarized in Table 1.

One important result deduced from the SLS fitting is that $N_{agg/L}$ ($\approx$ 3 chains/nm) remains constant as a function of the sonication time, which means that the inner structure of the micelle is preserved even after 40 min of sonication. This conclusion is also confirmed by a plot of $qR_\theta/\pi M_0 Kc$ as a function of qL, which generates a single master curve for the data as shown in Figure S1 in Supporting Information. This result also demonstrates that the weight-average length of the micelles remains proportional to their weight-average molecular weight, according to the equation $M_w = L_w M_0 N_{agg/L}$, where M_0 is the weight-average molecular weight of PI-*b*-PFS block copolymer. The relationship between M_w and L_w is thus $M_w = 96\,000\ L_w$. We conclude that, as in the case of double-stranded DNA,[19] micelle scission occurs perpendicular to the micelle axis.

(51) Ballauff, M.; Wolf, B. A. *Macromolecules* **1981**, *14*, 654–658.
(52) Davis, A. W.; Phillips, D. R. *Biochem. J.* **1978**, *173*, 179–183.
(53) Pritchard, N. J.; Hugues, D. E.; Peacocke, A. R. *Biopolymers* **1966**, *4*, 259–273.
(54) Peacocke, A. R.; Pritchard, N. J. *Biopolymers* **1968**, *6*, 605–623.
(55) Hall, C. E.; Doty, P. *J. Am. Chem. Soc.* **1958**, *80*, 1269–1274.
(56) Wegner, A.; Savko, P. *Biochemistry* **1982**, *21*, 1909–1913.
(57) Stathopulos, P. B.; Scholz, G. A.; Hwang, Y.; Rumfeldt, J. A.; Lepock, J. R.; Meiering, E. M. *Protein Sci.* **2004**, *13*, 3017–3027.
(58) Ban, T.; Yamaguchi, K.; Goto, Y. *Acc. Chem. Res.* **2006**, *39*, 663–670.
(59) Yan, X.; Liu, G. *Langmuir* **2004**, *20*, 4677–4683.

Table 2. Main Characteristics Determined by TEM for Micelle Samples

sonication time	0 s	10 s	30 s	60 s	150 s	240 s	10 min	20 min	40 min
L_n (nm)	1050	530	450	335	260	205	140	120	110
L_w (nm)	2080[a]	990	775	470	400	290	190	160	150
PDI	2	1.9	1.7	1.4	1.5	1.4	1.4	1.4	1.4

[a] Obtained from analysis of the data in Figure 3B in terms of eq 1. From the Gaussian fit to the main peak in Figure 3B, we obtained $L_w^{Gauss} = 2450$ nm.

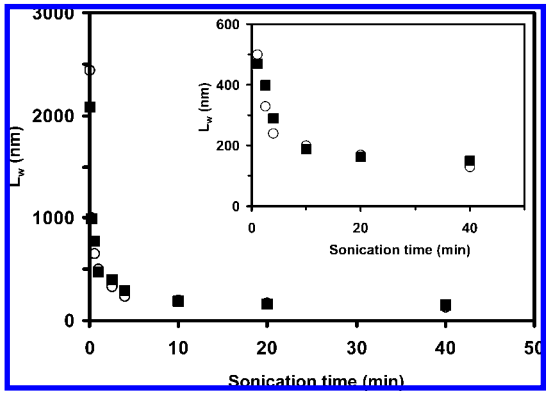

Figure 6. Plot of the micelle weight-average length as a function of sonication time for PI_{264}-*b*-PFS_{48} micelles in hexane ($c = 0.06$ mg/mL) as determined by TEM image analysis (■) and by SLS (○). The inset shows the evolution of L_w on an expanded y-axis scale, and omits the first two data points at 0 and 10 s.

The fact that $N_{agg/L}$ is not affected by the sonication time also suggests that the block copolymer is not degraded during the process.

TEM Studies of Micelle Scission. Samples for TEM analysis were taken from the solutions after each sonication time. We used image analysis to evaluate the number and weight distribution of micelle length and calculated the number-average lengths, L_n, and weight-average lengths, L_w, of the micelles. These values for each sonication time are summarized in Table 2.

In Figure 6, we compare the weight-average lengths of the micelle deduced from TEM image analysis and from the fit of the SLS data as a function of sonication time. From this plot, one can see that both techniques are in excellent agreement, which confirms the quality of the SLS results. It is interesting to note how fragile these micelles are: after only 10 s of sonication, the weight-average length of the micelles is lowered by a factor of 2. It appears also that the weight-average length of the sonicated micelles reaches a plateau value close to $L_w =$ 140 nm after 10 min of sonication, which would suggest that under the experimental conditions employed, the micelles cannot be broken into smaller pieces, similar to the results reported for sonicated DNA.[52] However, when we plot L_w against log time (see Figure S2 in Supporting Information), as suggested by a reviewer, one sees no indication of a plateau but rather a slowing down of the scission process as the micelles become shorter.

Modeling Micelle Scission under Sonication. In ref 9 we reported that solutions of very similar PI-*b*-PFS block copolymer micelles, even after sonication, retained their length and CLD when they were aged in the dark for several months at room temperature. This finding gives us confidence that the fragments produced during sonication will not recombine during the measurements used to determine their CLD. The stability of the fragments, in combination with the narrow length distribution of the initial sample, makes it possible to compare these experimental length distributions with the predictions of models previously applied to the degradation by sonication of polymer molecules and DNA. These models assume that the degradation rate is first-order in the concentration of micelles, with an individual rate constant k_i for the degradation of micelles with length L_i. Individual rate constants k_{ij} can be defined for the scission of a micelle of length L_i into two shorter cylinders with j and $i - j$ subunits. The value of k_i is given by the sum over all k_{ij} of micelles of length L_i (i.e., containing i subunits):

$$k_i = \sum_{j=1}^{i-1} k_{i,j} \tag{5}$$

$$\frac{dn_i}{dt} = -\left(\sum_{j=1}^{i-1} k_{i,j}\right) n_i + (k_{i+1,1} + k_{i+1,i}) n_{i+1} + \cdots + (k_{r,i} + k_{r,r-i}) n_r \tag{6}$$

where dn_i/dt is the "reaction" rate of the micelles of length L_i, n_i is the number of micelles of length L_i, and r is the aggregation number of the longest micelle. The parameter n_i can be expressed as a vector:

$$\vec{n} = \begin{pmatrix} n_1 \\ n_2 \\ \vdots \\ n_r \end{pmatrix} \tag{7}$$

with

$$\frac{d\vec{n}}{dt} = \mathbf{A}\vec{n} \tag{8}$$

$$\mathbf{A} = \begin{pmatrix} 0 & k_{2,1} + k_{2,1} & k_{3,1} + k_{3,2} & \cdots & k_{r,1} + k_{r,r-1} \\ 0 & -k_{2,1} & k_{3,2} + k_{3,1} & \cdots & k_{r,2} + k_{r,r-2} \\ 0 & 0 & -\sum_{j=1}^{2} k_{3,j} & \cdots & k_{r,3} + k_{r,r-3} \\ 0 & 0 & 0 & \ddots & \vdots \\ 0 & 0 & 0 & 0 & -\sum_{j=1}^{r-1} k_{r,j} \end{pmatrix} \tag{9}$$

Following Ballauff and Wolf,[24] we transformed the system of differential equations into an eigenvalue problem (eqs 8 and 9), where **A** is the matrix of kinetic coefficients, typical of a mode of scission. Matrix **A** is an upper triangular matrix, due to the fact that there is no recombination of the micelles after fragmentation. We used the knowledge of **A** and of the starting conditions (the number distribution of the micelle length at time $t = 0$) to calculate the number distribution of the micelle length at any time. The weight distributions in micelle length were then calculated from the number distribution and compared to the weight distributions evaluated from TEM image analysis.

Computations were performed by a program written to run on Matlab software, developed by Mathworks Inc., Natick, MA. Three different matrices, **A**, were then defined, corresponding to three different modes of scission.

For each sample, we first plotted the weight distribution of the micelle length, and then we simulated the mode of scission using three scission models. Model I is the random scission model. In this model, all rupture sites have the same probability of breaking, and the scission rate k of a bond is independent of the micelle length. The scission probability is expressed as

$$k_{ij} = k \qquad \text{for } i \le j \tag{10a}$$

$$k_{ij} = 0 \qquad \text{for } i \ge j \tag{10b}$$

$$k_{jj} = -\sum_{i=1}^{j-1} k_{ij} = -k(j-1) \tag{10c}$$

Model II is the central scission model. In this model, micelles are split only at half their length. In this model it is possible to consider that the scission rate depends on the length of the micelle. For this case, we used the model as defined by Ballauff and Wolf:[24]

i odd

$$k_{ij} = k(j-1)^x \qquad \text{if } i = (j-1)/2 \tag{11a}$$

$$k_{ij} = 0 \qquad \text{if } i \neq (j-1)/2 \tag{11b}$$

i even

$$k_{ij} = 0.5\, k\, (j-1)^x \qquad \text{if } i = (j-1)/2 \pm 0.5 \tag{11c}$$

$$k_{ij} = 0 \qquad \text{if } i \neq (j-1)/2 \pm 0.5 \tag{11d}$$

$$k_{jj} = -\sum_{i=1}^{j-1} k_{ij} = -k(j-1)^x \tag{11e}$$

where x describes the dependence of the degradation rate on the length of the micelle.

Model III is the Gaussian model. In this model, the probability of micelle scission is assumed to be Gaussian about the midpoint of the micelle. A broad Gaussian distribution approaches the random scission model, whereas an extremely narrow Gaussian distribution leads to the central chain scission model:

$$k_{ij} = k(j-1)^x \frac{1}{\sigma_j (2\pi)^{1/2}} \exp\left[-\left(i - \frac{j}{2}\right)^2 / 2\sigma_j^2\right] \qquad \text{for } i \le j \tag{12a}$$

$$k_{ij} = 0 \qquad \text{for } i \ge j \tag{12b}$$

$$k_{jj} = -\sum_{i=1}^{j-1} k_{ij} = -k(j-1)^x \tag{12c}$$

where $\sigma_j = jR$. When $x = 1$ and $R > 10$, model III approaches the case of random scission, whereas when $R < 0.05$, model III approaches the case of central scission, and the micelles break at their centers.

The scission rate at a given site should not depend upon the sonication time. The constant k must then be unique for all sonication times and must be evaluated by minimizing the sum S:

$$S = \sum_{t_s} \left\{ \sum_{i}^{250} \left[n_i^{\text{calcd}}(t_s) - n_i^{\text{exp}}(t_s) \right]^2 \right\} \tag{13}$$

where t_s are the different sonication times (10 s, 30 s, 60 s, 150 s, 240 s, 10 min, 20 min, and 40 min); n_i^{exp} and n_i^{calcd} are the number of micelles of weight length L_{wi} as determined experimentally (n_i^{exp}) and by simulation (n_i^{calcd}).

In Figure 7 we compare the simulated weight-average lengths of the micelles in the sonicated solutions (as calculated with the three different models) to the weight-average length evaluated from the TEM image analysis. We can see that, in all cases, the simulated weight-average length follows the same trend as L_w evaluated experimentally: a monotonic decrease of L_w as a function of sonication time. No other adjustable parameter was used to enhance the quality of the fit in the case of the random scission model. The parameter x was optimized in fitting data to the central scission model, and the parameters x and R were used as fitting parameters for the Gaussian scission model. The parameter x accounts for a possible influence of the micelle length on the breakage rate of the micelles, and the magnitude of R indicates the location of the breaking sites along the micelle (small R means that the scission occurs primarily in the centers of the micelles, whereas larger R values indicate that the scission occurs anywhere along the structure). The best fits to the data in Figure 6 were obtained with $x = 2$ for the central scission model and with $x = 2.6$ and $R = 1$ for the Gaussian scission model.

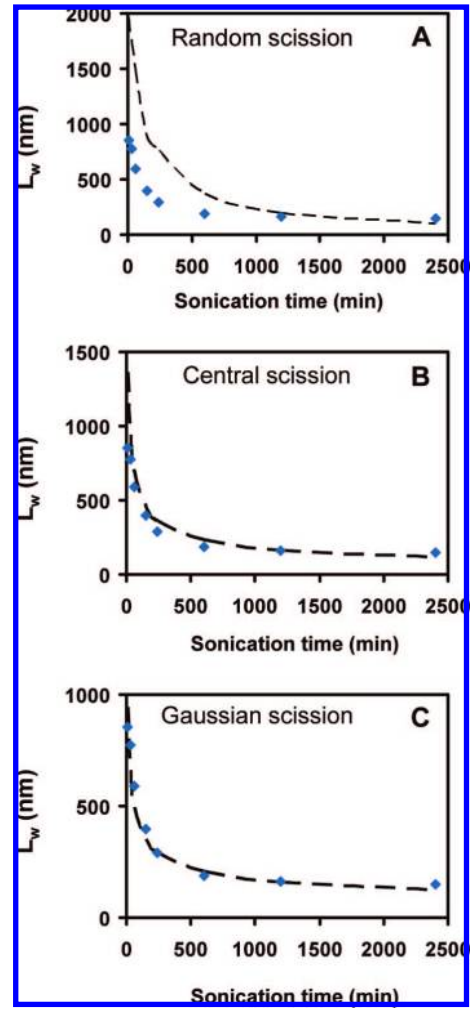

Figure 7. Weight-average length of PI_{264}-*b*-PFS_{48} sonicated micelle solutions as a function of sonication time as evaluated by TEM image analysis (blue diamonds) and as simulated (− − −) by use of (A) the random scission model, (B) the central scission model (with $x = 2$), or (C) the Gaussian scission model (with $x = 2.6$ and $R = 1$).

While the weight-average lengths of the sonicated micelles deduced from the central and Gaussian scission models are in good agreement with the experimental data, the weight-average lengths of the micelles deduced from the random scission model are too large at short sonication times. This discrepancy between the experimental data and the random scission model is representative of any model that does not account for the strong dependence of the fracture rate on the overall micelle length. To emphasize this fact, we compared the measured L_w values with the predictions of the central scission model with a fixed value of $x = 1$ and to the Gaussian scission model with fixed

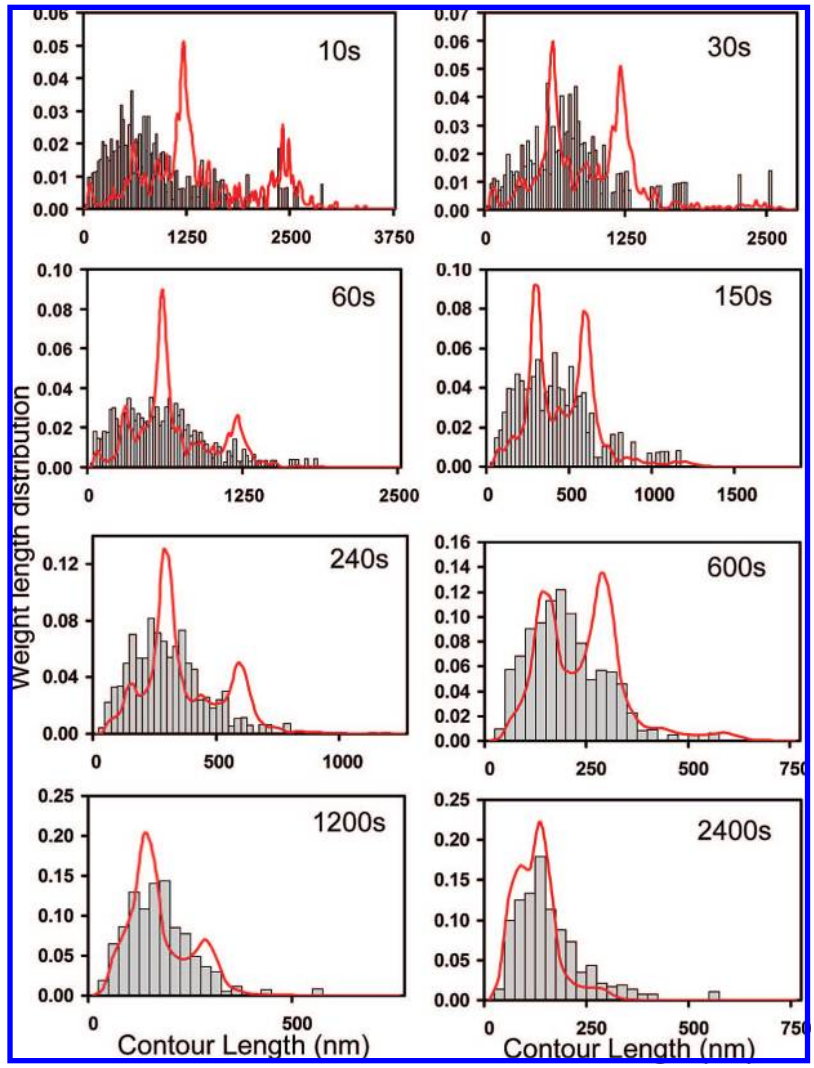

Figure 8. Weight length distribution of sonicated PI_{264}-*b*-PFS_{48} micelles as evaluated by analysis of TEM images (bars) and as simulated using the central scission model (curve), with $x = 2$. The sonication time is given for each graph. The initial weight distribution is shown in Figure 3B.

values of $x = 1$ and $R = 1$. The fits to the experimental data are poor. These plots are presented in Figure S3 in Supporting Information.

To differentiate between the central and the Gaussian scission models, we compare experimental weight length distributions with data simulated according to the central scission model (Figure 8) and the Gaussian scission model (Figure 9). The main feature of the experimental data is the presence of one broad peak at short sonication times, which moves to lower weight-average length values and narrows when the sonication time increases.

Central Scission Model. Comparison of the measured chain length distributions presented in Figure 8 with data simulated according to the central scission model show poor agreement with the model. The data at 10 s sonication time show a glaring inconsistency with the model, predicting three sharp peaks in the distribution. The first peak is centered at 2.5 μm, which corresponds to unbroken micelles; the second peak is at 1.25 μm, half the weight-average length of the starting material; and a third peak is centered at around 600 nm. Such sharp peaks in the simulated data are due to the fact that the starting weight length distribution was very narrow, a consequence of the narrow distribution of micelles prior to sonication. At later times, the disagreement is less pronounced, and the "best fit" to the experimental data was obtained for $x = 2$ ($S = 0.14$).

Gaussian Scission Model. The experimental weight length distribution following sonication of the PI_{264}-*b*-PFS_{48} micelles is compared to the predictions of the Gaussian scission model in Figure 9. The best fit was obtained for $x = 2.6$ and $R = 1$ ($S = 0.03$), and the rate constant k was equal to 9×10^{-6} s^{-1}. For most of the sonication times, the experimental and simulated distributions are in excellent agreement. This agreement, however, was obtained using a very large value for x (2.6), implying a very strong dependence of the fragmentation rate on the length of the micelles. This value is much larger than values reported for fragmentation of polymer chains or of DNA molecules subjected to sonication.[19,24] This high sensitivity to ultrasound might be explained by the high aspect ratio of the micelles, which increases the fragility of the structure to shear stress. Fracture leads to shorter structures with a smaller aspect ratio and less sensitivity to applied stress fields.

Summary

We have described the formation of fiberlike micelles in hexane with a very narrow weight-average distribution of lengths ($L_w = 2500$ nm) and the nature of their fragmentation following

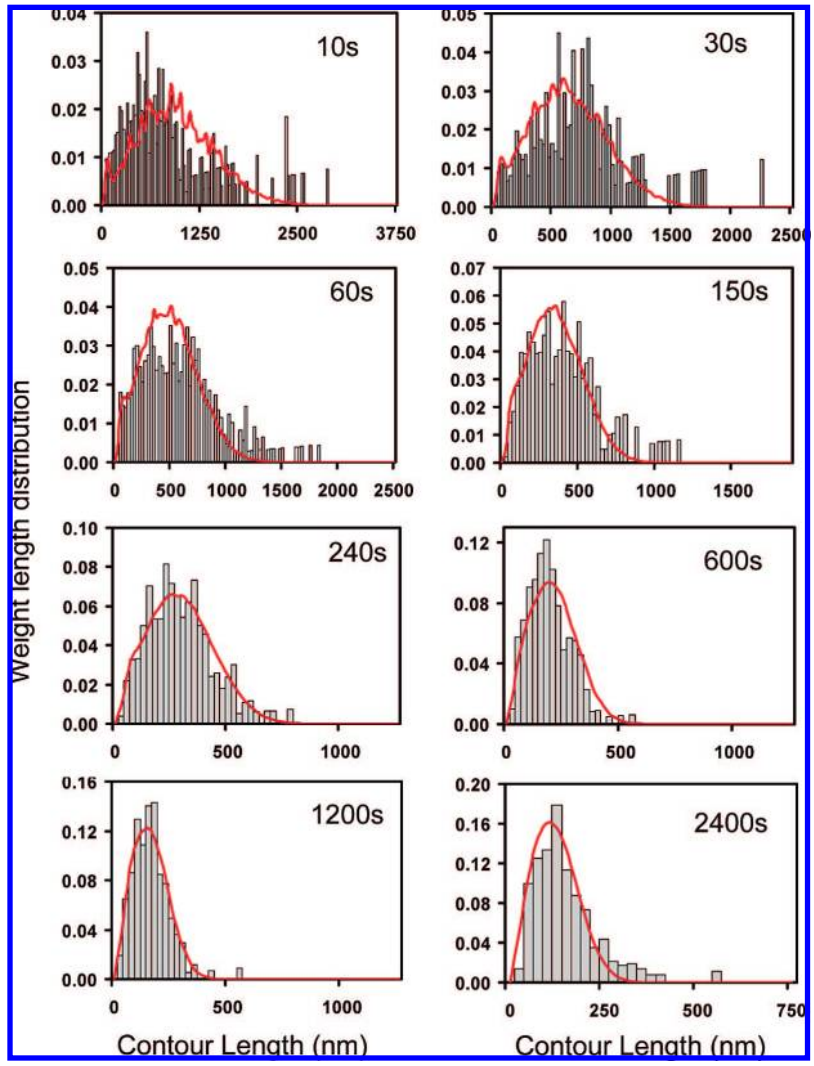

Figure 9. Weight length distribution of sonicated PI_{264}-*b*-PFS_{48} micelles as evaluated by analysis of TEM images (bars) and as simulated by the Gaussian scission model (curve) with $x = 2.6$ and $R = 1$. The sonication time is given in each graph. The initial weight distribution is shown in Figure 3B.

exposure to ultrasound. The micelles were formed by heating a sealed solution of PI_{264}-*b*-PFS_{48} block copolymer to 80 °C followed by slow cooling back to room temperature. Static light scattering studies showed that, upon sonication, the micelles became shorter but maintained their mass per unit length, indicating fracture perpendicular to the long axis of the structure. At long sonication times, the micelle weight-average length decreases to a value close to 100 nm with a rather low dispersion in length. More detailed information is available from analysis of TEM images of the sonicated micelles. Simulations show that micelle scission follows a Gaussian model, with a slight preference for fragmentation near the centers of the structures and without recombination of the fragments. The fitting parameters indicate that long micelles are easily broken whereas short micelles are more stable. The scission of PI_{264}-*b*-PFS_{48}-based micelles shows some similarity with DNA cleavage, in that both break perpendicularly to their main axis and reach a finite length at long sonication times. However, scission of fiberlike micelles depends much more strongly on the micelle length than that of DNA. We attribute this behavior both to the rigidity of the structures and to their large aspect ratio.

In the Introduction, we drew an analogy between the nature of fiberlike PFS block copolymer micelles and amyloid fibers studied by others. Both have similar dimensions with high aspect ratios, and both types of structures undergo bidirectional growth by (epitaxial) deposition of soluble macromolecules onto the ends of existing fibers or fiber fragments. The amyloid fibers are also very sensitive to fragmentation when exposed to ultrasound. The results reported here suggest that these fibers should also rupture according to a Gaussian fragmentation model and exhibit a fracture rate that is very sensitive to fiber length.

Acknowledgment. We thank Natural Sciences and Engineering Research Council of Canada for their support of this research. I.M. thanks the European Union for the Marie Curie Chair and the Royal Society for a Wolfson Research Merit Award. The authors thank Professors T. Scheibel and S. L. Lindquist for the image reproduced in Figure 1A.

Supporting Information Available: All experimental details, a normalized Holtzer−Casassa plot of the light scattering data, a plot of L_w against log time, and additional plots of experimental and simulated weight-average lengths of the micelles as a function of sonication time. This material is available free of charge via the Internet at http://pubs.acs.org.

JA805262V